Throughput Maximization for Intelligent Refracting Surface Assisted mmWave High-Speed Train Communications

Jing Li, Yong Niu, *Member, IEEE,* Hao Wu, *Member, IEEE,* Bo Ai, *Fellow, IEEE,* Ruisi He, *Senior Member, IEEE,* Ning Wang, *Member, IEEE,* Sheng Chen, *Fellow, IEEE*

***Abstract*—With the increasing demands from passengers for data-intensive services, millimeter-wave (mmWave) communication is considered as an effective technique to release the transmission pressure on high speed train (HST) networks. However, mmWave signals encounter severe losses when passing through the carriage, which decreases the quality of services on board. In this paper, we investigate an intelligent refracting surface (IRS)-assisted HST communication system. Herein, an IRS is deployed on the train window to dynamically reconfigure the propagation environment, and a hybrid time division multiple access-nonorthogonal multiple access scheme is leveraged for interference mitigation. We aim to maximize the overall throughput while taking into account the constraints imposed by base station beamforming, IRS discrete phase shifts and transmit power. To obtain a practical solution, we employ an alternating optimization method and propose a two-stage algorithm. In the first stage, the successive convex approximation method and branch and bound algorithm are leveraged for IRS phase shift design. In the second stage, the Lagrangian multiplier method is utilized for power allocation. Simulation results demonstrate the benefits of IRS adoption and power allocation for throughput improvement in mmWave HST networks.**

***Index Terms*—Millimeter-wave, intelligent refracting surface, hybrid time division multiple access-nonorthogonal multiple access, phase shift design, power allocation.**

I. Introduction

As an efficient, green and eco-friendly transport mode, high-speed train (HST) has attracted worldwide attention in the past two decades. By 2022, the total millage of HST rail lines, with the speed of train exceeding 200 km/h, has reached 56,000 km and is expected to double in 30 years [1]. In many countries, like China and Spain, HSTs link the major city clusters, fasten long-distance travel, and are changing people's mobility habits deeply. Fast growing number of passengers has demanded much stricter safe operation as well as multimedia services from railway systems, which powers the sustainable development of wireless communications for HST systems [2]. Initially, the Global System for Mobile Communications Railway [3] provisioned services of voice communications and control signaling transmission but failed to satisfy personal broadband applications. To handle this problem, Long Term Evolution for Railway [3] was introduced at the beginning of 2010s, which supports megabits-per-second order data rate but it still does not meet the requirements of massive connectivity and intensive data exchange for the future HST system [2], [3]. The fifth-generation (5G) technologies are expected to ensure real-time and high-quality transmissions for both passengers and railway operation messages, to start a new era in HST communications [4].

Exploiting millimeter-wave (mmWave) communications, 5G for Railway [5] has the potential to offer multimedia services that require multi-gigabit rate, e.g., video conference, live broadcast, online gaming, etc., thereby enhancing the customer experience. In addition, mmWave integrated with multiple-input multiple-output (MIMO) and beamforming techniques is capable of offering comprehensive perception, interconnection, and information interaction among railway users and infrastructures, which subsequently contributes to the construction of intelligent transportation system (ITS) [5]. However, given the propagation characteristics of mmWave signals and dynamic nature of railway scenarios, there are many challenges to overcome in order to maintain high-quality on-board services. Specifically, experiencing severe path loss, the coverage radius of mmWave is limited, and frequent handover occurs in train-to-ground (T2G) communications. Moreover, mmWave signals suffer from serious penetration loss when passing through solid materials, including glasses, metals and trees, and consequently they are vulnerable to blockage [6]. During mobility, the quality of services (QoS) degrades significantly once line-of-sight (LoS) links between passengers and the base station (BS) are blocked by the carriage or other obstacles [7]. To this end, many researchers deploy mobile relay stations (MRSs) on the train to combat penetration loss and control handover, whereas MIMO technologies are typically involved as well [3], [8], [9]. These solutions, however, require extra hardware cost and energy consumption, while introducing transmission delay.

Fortunately, the authors of [10] have confirmed the feasibility of adopting intelligent refracting surface (IRS) in future wireless communications, which provides a new means to improve the QoS and energy efficiency of HST communications [11], [12]. Specifically, by adjusting the coefficient of each refractive element, the propagation channel is reconfigured dynamically to enable robust wireless links, serving

Jing Li, Yong Niu, Hao Wu, Bo Ai and Ruisi He are with the State Key Laboratory of Rail Traffic Control and Safety, Beijing Jiaotong University, Beijing 100044, China, and also with Beijing Engineering Research Center of High-speed Railway Broadband Mobile Communications, Beijing 100044, China (E-mails: jinglee@bjtu.edu.cn, niuy11@163.com, hwu@bjtu.edu.cn, boai@bjtu.edu.cn, ruisi.he@bjtu.edu.cn.

Ning Wang is with School of Information Engineering, Zhengzhou University, Zhengzhou 450001, China (E-mail: ienwang@zzu.edu.cn).

Sheng Chen is with School of Electronics and Computer Science, University of Southampton, Southampton SO17 1BJ, UK (E-mail: sqc@ecs.soton.ac.uk).

This study is supported by the State Key Laboratory of Rail Traffic Control and Safety under Grant No. RCS2021ZT008.

as a promising technique to extend the coverage inside the train and improve communication quality without extra power consumption [13]. Inspired by this, we consider enhancing the throughput of downlink HST communications by a window-deployed IRS, which refracts incident signals to users on board during mobility. Under the condition that the channel state information (CSI) remains unchanged in one frame but can vary from frame to frame, we can update the system design dynamically. Note that the amplitude gain at IRS is neglected since signals experience severe penetration loss when passing through the window anyway. Moreover, to eliminate transmission interference and fully exploit the effect of IRS, both clustering and hybrid transmission techniques [14], [15] are leveraged. The main contributions of this paper are summarized as follows.

- We study an IRS-assisted hybrid time division multiple access (TDMA)-nonorthogonal multiple access (NOMA) mmWave HST communication system, where a transparent IRS is deployed to assist T2G communications. Based on the practical position-prediction model and channel model, we formulate the throughput maximization problem that takes into account the constraints on BS beamforming, IRS refraction and transmit power.
- We propose a two-stage optimization algorithm to solve this optimization. Specifically, first we alternately optimize beamforming and IRS phase shift in each frame, where the maximum ratio combining (MRT), successive convex approximation (SCA) and branch and bound (BB) algorithm are utilized. Based on these optimization results and by incorporating the characteristics of high-speed mobility, we perform local power allocation in every fixed interval, to improve the overall throughput effectively.
- By comparing the achievable performance of the proposed algorithm with other existing schemes given different numbers of users, IRS sizes, Rician K-factors and quantization bits, the simulation results reveal the effectiveness of IRS adoption and power allocation for throughput improvement in the HST scenario.

The remainder of this paper is organized as follows. Section II summarizes the related work. Section III introduces the system model and then formulates the throughput maximization problem. In Section IV, a two-stage solution is proposed based on alternating optimization and Lagrangian multiplier method. Simulation results and discussions are presented in Section V. Finally, Section VI concludes the paper.

II. Related Work

Recently, the research in applying reconfigurable intelligent surfaces (RISs) to HST networks has attracted increasing interests. For example, the authors of [14] employed an RIS-assisted approach to increase the anti-interference capability of railway wireless communication systems that require ultra high reliability. Likewise, base on the deep reinforcement learning, Xu and Ai [15] optimized the BS beamforming and RIS phase shifts to enhance the resilience of mmWave HST networks. The work [16] proposed a RIS-assisted unmanned aerial vehicle scheme to provide stable communication services for HST users, demonstrating its superior performance in obstacle avoidance and resource utilization. Based on the statistical CSI, the study [17] jointly designed the beamforming and RIS phase shift matrix in the downlink of mmWave MIMO HST system to reduce the outage probability. The work [18] presented a train-ground time division duplexing based wireless mobile communication design with double RISs deployed at both BS and MRS sides, to achieve significant performance gain in uplink transmission. Typically, most existing works leverage the reflecting mode of RISs to assist HST communications, which enhances the system performance to some extent but fails to resolve the challenging problem of signal attenuation caused by train carriages.

As a new type of RIS, the emerging IRS offers a new paradigm for mobile communications. Initially, efficient refractive metasurfaces were designed based on physical property requirements in [19], [20], paving the way for IRS solutions. Furthermore, the authors of [13] implemented optically transparent metasurfaces to expand the mmWave coverage, which can be attached to existing walls and glass windows. IRS is capable of aiding mobile communications in vehicular networks. For example, the work [21] successfully deployed the IRS on a moving vehicle for enhancing the transmission rate and reliability between in-vehicle users and the roadside BS by channel estimation and refraction optimization. To date, few works have noted IRS-assisted HST communications. The study [7] investigated the possibility of IRS solutions to address the mobility characteristics and design challenges of HST networks, and verified the benefits of adopting IRSs to HST communications. Likewise, the authors of [22] presented a low-complexity channel estimation method with Doppler shifts recovery, which is shown to be effective in ITS-assisted HST wireless communication systems. These limited efforts of applying IRSs however are still limited to channel design, and they seldom involve signal processing or resource management techniques for performance improvement.

III. System Model

We investigate the IRS-assisted mmWave HST communication system illustrated in Fig. 1, where I users on board are served by a track-side BS with L antennas. Since direct links are easily blocked during mobility, an IRS with M refractive

Fig. 1. IRS-assisted mmWave HST communication system.

elements is mounted on the train window to aid downlink power transfer and communications. A smart controller adjusts the IRS elements independently so as to enhance QoS on board and improve network throughput. For ease of exposition, we assume that the train runs at a constant speed of v and passes through the cell with a coverage radius of R in time $t = 2R/v$. In practice, users remain relative stationary with each other in a frame while the BS transmits data streams concurrently.

A hybrid TDMA-NOMA transmission scheme is leveraged to balance the complexity and performance. As such, I users are equally grouped into K clusters based on their requesting time, and N users in each cluster simultaneously access the network by employing NOMA. Denoting the duration of each TDMA frame as τ, different clusters communicate with the BS in an orthogonal TDMA manner. The communication distance and channel model are updated frame by frame, which are specified as follows.

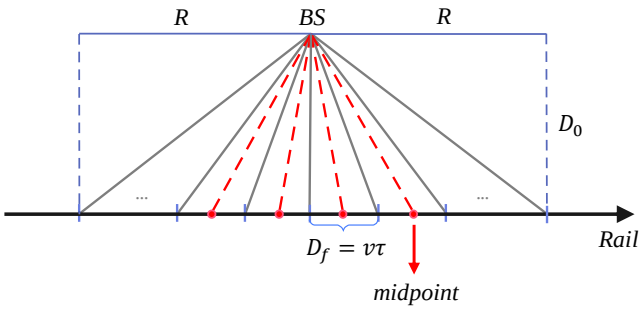

Fig. 2. The mobility trajectory of HST.

A. Distance-Prediction Model

Because of the short frame duration, it is reasonable to assume that the communication distance between the BS and the train remains approximately constant in a frame, but it changes from frame to frame. Therefore, we consider the mobility model illustrated in Fig. 2, where the distance from the BS to the rail is denoted by D_0, and the position of the train in frame k can be approximated with the midpoint of the corresponding segment. Thus, we estimate the distance between the BS and IRS in frame k, denoted as D_k, by

$$D_k = \begin{cases} \left(\left(R - (k - \frac{1}{2})D_f\right)^2 + D_0^2 \right)^{\frac{1}{2}}, & k \le \lfloor \frac{K}{2} \rfloor, \\ \left(\left((k - \frac{1}{2})D_f - R\right)^2 + D_0^2 \right)^{\frac{1}{2}}, & k > \lfloor \frac{K}{2} \rfloor, \end{cases} \tag{1}$$

with $D_f = v\tau$ denoting the distance advanced in a frame.

B. Channel Model

Consider a quasi-static fast fading channel, with the CSI remaining constant within a frame but changing in the subsequent frames [11]. The channel gains from the BS to the IRS and from the IRS to users are modeled as Rician fading, where the contribution of LoS and non-LoS (NLoS) multipath components are taken into account [23]. Specifically, in frame k, the BS-IRS channel gain matrix $\mathbf{G}_k \in \mathbb{C}^{M\times L}$ is given by

$$\mathbf{G}_k = \sqrt{\frac{K_f}{K_f+1}}\overline{\mathbf{G}}_k + \sqrt{\frac{1}{K_f+1}}\widehat{\mathbf{G}}_k, \tag{2}$$

where K_f denotes the Rician K-factor. In (2), $\overline{\mathbf{G}}_k \in \mathbb{C}^{M\times L}$ represents the LoS component given by

$$\overline{\mathbf{G}}_k = \sqrt{h_0 D_k^{-\beta_1}} \begin{bmatrix} \alpha_k\left(\phi^A_{1,1}, \omega^A_{1,1}\right) & \dots & \alpha_k\left(\phi^A_{1,L}, \omega^A_{1,L}\right) \\ \vdots & \ddots & \vdots \\ \alpha_k\left(\phi^A_{M,1}, \omega^A_{M,1}\right) & \dots & \alpha_k\left(\phi^A_{M,L}, \omega^A_{M,L}\right) \end{bmatrix}, \tag{3}$$

where $\alpha_k(\cdot,\cdot)$ denotes the array response, $\phi^A_{m,l}$ and $\omega^A_{m,l}$ are the azimuth and elevation angles-of-arrival (AoAs), respectively, from the l-th BS antenna to the m-th IRS element at frame k, and h_0 is the reference path loss at distance of 1 m, while β_1 is the path loss exponent. As aforementioned, D_k is the distance between the BS and IRS, kept fixed in frame k. Moreover, $\widehat{\mathbf{G}}_k \in \mathbb{C}^{M\times L}$ represents the NLoS component matrix, whose elements follow the complex normal distribution with zero mean and unit variance [24].

Similarly, the LoS component of the channel gain vector $\mathbf{v}^{\mathrm{T}}_{k,i} \in \mathbb{C}^{1\times M}$ from the IRS to user i in frame k is given by

$$\overline{\mathbf{v}}^{\mathrm{T}}_{k,i} = \sqrt{h_0 d_{k,i}^{-\beta_2}}\left[\alpha_{k,i}\left(\phi^D_{1,1}, \omega^D_{1,1}\right), \dots, \alpha_{k,i}\left(\phi^D_{1,M}, \omega^D_{1,M}\right)\right], \tag{4}$$

where $d_{k,i}$ is the distance between the IRS and the i-th user, β_2 denotes the path loss exponent insider the carriage, $\phi^D_{1,m}$ and $\omega^D_{1,m}$ are the azimuth and elevation angles of departure (AoDs), respectively, from the m-th IRS element to the i-th user. The elements of the NLoS component vector $\widehat{\mathbf{v}}^{\mathrm{T}}_{k,i} \in \mathbb{C}^{1\times M}$ also follow the complex normal distribution with zero mean and unit variance.

We assume that the perfect CSI for BS to IRS and IRS to users are available. Since refracting elements have no digital processing ability, we perform digital beamforming at the BS and analog beamforming at the IRS. Denote the transmit signal for user j, BS beamforming vector, IRS phase shift vector in frame k by $s_{k,j}$, $\mathbf{f}_k \in \mathbb{C}^{L\times 1}$ and $\mathbf{\Theta}_k = \mathrm{diag}\left(e^{\mathrm{j}\psi_{k,1}}, \dots, e^{\mathrm{j}\psi_{k,M}}\right)$. The received signal for user i can be expressed as

$$\begin{aligned} r_{k,i} =& \mathbf{v}^{\mathrm{T}}_{k,i}\mathbf{\Theta}_k\mathbf{G}_k\mathbf{f}_k \sum_{j=1}^{N}\sqrt{P_k}s_{k,j} + w_i = \underbrace{\mathbf{v}^{\mathrm{T}}_{k,i}\mathbf{\Theta}_k\mathbf{G}_k\mathbf{f}_k\sqrt{P_k}s_{k,i}}_{\text{desired signal}} \\ &+ \underbrace{\sum_{j=1, j\neq i}^{N}\mathbf{v}^{\mathrm{T}}_{k,i}\mathbf{\Theta}_k\mathbf{G}_k\mathbf{f}_k\sqrt{P_k}s_{k,j}}_{\text{user interference}} + w_i, \end{aligned} \tag{5}$$

where P_k is the transmit power in frame k, and w_i is the additive white Gaussian noise (AWGN) at user i, with zero mean and variance σ^2, and $E\left[|s_{k,j}|^2\right] = 1$, $\forall k, j$.

By exploiting the successive interference cancellation enabled NOMA, N users can be multiplexed on the same channel [25], [26], and the SINR received by user i in frame k can be written as

$$\gamma_{k,i} = \frac{P_k\left|\mathbf{v}^{\mathrm{T}}_{k,i}\mathbf{\Theta}_k\mathbf{G}_k\mathbf{f}_k\right|^2}{\sum_{j=i+1}^{N}P_k\left|\mathbf{v}^{\mathrm{T}}_{k,j}\mathbf{\Theta}_k\mathbf{G}_k\mathbf{f}_k\right|^2 + \sigma^2}, \tag{6}$$

The aggregate achievable data rate in frame k is given by [27]

$$R_k = \sum_{i=1}^{N} \log_2 \left(1+\gamma_{k,i}\right) = \log_2 \left(1+\sum_{i=1}^{N} \frac{P_k \left|\mathbf{v}_{k,i}^{\mathrm{T}} \mathbf{\Theta}_k \mathbf{G}_k \mathbf{f}_k\right|^2}{\sigma^2}\right). \quad (7)$$

C. Problem Formulation

First we recap the system configuration and parameters. The BS has L antennas, and the IRS has M refractive elements. The system supports I users, and they are divided equally into K clusters, each having N users, i.e., $I = KN$. The time duration t is divided into K TDMA frames, each having the duration of τ, i.e., $t = K\tau$. Each group is assigned with a distinct frame, and the N users of the same group share the same frame. Furthermore, the total transmit power over time duration t is set to P_{sum}. Each refractive element $\theta = e^{\mathrm{j}\psi}$ of the IRS can take the value from the set of 2^e values, namely, the phase shift $\psi = \frac{2\pi a}{2^e-1}$, $a \in \{0, 1, \ldots, 2^e-1\}$, with the magnitude $\|\theta\| = 1$, where e denotes the quantization bits. We also define the transmit power vector over the K TDMA frames by $\mathbf{p} = \left[P_1, \ldots, P_K\right]^{\mathrm{T}}$.

Our goal is to maximize the overall throughput in time duration t by jointly optimizing the beamforming, IRS phase shift and power allocation. The problem is defined as

$$\mathcal{P}: \max_{\mathbf{p}, \{\mathbf{\Theta}_k\}_{k=1}^K, \{\mathbf{f}_k\}_{k=1}^K} \sum_{k=1}^{K} \frac{\tau}{t} R_k, \quad (8)$$

$$\text{s.t.} \ \sum_{k=1}^{K} P_k = P_{\mathrm{sum}}, \quad (9)$$

$$0 \le P_k \le P_{\mathrm{sum}}, \ \forall k, \quad (10)$$

$$\mathbf{f}_k^{\mathrm{H}} \mathbf{f}_k \le 1, \ \forall k, \quad (11)$$

$$\psi_{k,m} = \frac{2\pi a}{2^e-1}, a \in \{0, 1, \ldots, 2^e-1\}, \ \forall k, m, \quad (12)$$

$$\left\|\theta_{k,m}\right\| = 1, \ \forall k, m. \quad (13)$$

The constraints (9) and (10) limit the total power consumption to P_{sum}, which is the upper bound of power allocated to each cluster. Next (11) imposes a magnitude constraint on each beamforming vector, while (12) specifies the discrete set from which the phase shift of each element takes value, and (13) imposes the unit amplitude constraints on IRS elements.

IV. Throughput Maximum Algorithm

In the joint optimization problem $\mathcal{P}$, the optimization variables in the objective function are coupled while the constraints in (13) are non-convex. Thus there exists no standard method to solve $\mathcal{P}$ directly. We propose a two-stage optimization algorithm by leveraging problem decoupling and alternating optimization. In the first stage, we exploit MRT in beamforming design and optimize the phase shifts, while in the second stage we adjust the power allocated to each frame with the optimization results obtained in the first stage, to maximize the total throughput.

A. Stage One: Joint Optimization of Beamforming and IRS Phase Shifts

In this stage, we fix the power allocated to each frame to $\overline{P} = P_{\mathrm{sum}}/K$ and make the overall power allocation as $\overline{\mathbf{p}} = \left[\overline{P}, \overline{P}, \ldots, \overline{P}\right]$. With the power allocation vector $\mathbf{p}$ fixed to $\overline{\mathbf{p}}$, the optimization $\mathcal{P}$ is simplified to

$$\mathcal{P}1: \max_{\{\mathbf{\Theta}_k\}_{k=1}^K, \{\mathbf{f}_k\}_{k=1}^K} \sum_{k=1}^{K} \frac{\tau}{t} R_k \quad (14)$$

$$\text{s.t.} \ \mathbf{f}_k^{\mathrm{H}} \mathbf{f}_k \le 1, \ \forall k, \quad (15)$$

$$\psi_{k,m} \in [0, \ 2\pi], \ \forall k, m, \quad (16)$$

$$\left\|\theta_{k,m}\right\| = 1, \ \forall k, m. \quad (17)$$

Note that we have relaxed the phase shift of each refractive element to be a continuous variable taking value in $[0, \ \pi]$. To avoid high complexity of the joint optimization over the beamforming and IRS phase shifts, we further decouple $\mathcal{P}1$ into the two sub-problems, each involving one set of variables only with the other fixed, and an alternating algorithm is adopted to alternately optimize the transmit beamforming and the IRS phase shifts until converges.

1) Beamforming Optimization at BS: Given $\mathbf{p} = \overline{\mathbf{p}}$ and the set of $\{\mathbf{\Theta}_k\}_{k=1}^K$, the objective function of $\mathcal{P}1$ is monotonically increasing with the aggregate signal to noise ratio (SNR) of each cluster. Therefore, the optimization over $\{\mathbf{f}_k\}_{k=1}^K$ can be equivalently solved by maximizing the SNR of each cluster, where the optimal beamforming vectors can be obtained by solving the following K sub-problems

$$\mathcal{P}1_{\mathbf{f}_k}: \max_{\mathbf{f}_k} \sum_{i=1}^{N} \frac{\overline{P} \left|\mathbf{v}_{k,i}^{\mathrm{T}} \mathbf{\Theta}_k \mathbf{G}_k \mathbf{f}_k\right|^2}{\sigma^2}, \quad (18)$$

$$\text{s.t.} \ \mathbf{f}_k^{\mathrm{H}} \mathbf{f}_k \le 1, \quad (19)$$

for $1 \le k \le K$. Although $\mathcal{P}1_{\mathbf{f}_k}$ is non-convex with respect to $\mathbf{f}_k$, the closed-form optimal solution can be driven by

$$\mathbf{f}_k^{\star} = \sum_{i=1}^{N} \frac{\left(\mathbf{v}_{k,i}^{\mathrm{T}} \mathbf{\Theta}_k \mathbf{G}_k\right)^{\mathrm{H}}}{\left\|\mathbf{v}_{k,i}^{\mathrm{T}} \mathbf{\Theta}_k \mathbf{G}_k\right\|}, \quad (20)$$

which enables the MRT [28], [29].

2) IRS Phase Shift Design: Given the power allocation $\overline{\mathbf{p}}$ and the beamforming vectors $\{\mathbf{f}_k\}_{k=1}^K$, the optimization of the IRS phase shifts can be simplified as

$$\mathcal{P}1_{\mathbf{\Theta}}: \max_{\{\mathbf{\Theta}_k\}_{k=1}^K} \sum_{k=1}^{K} \frac{\tau}{t} R_k \quad (21)$$

$$\text{s.t.} \ \ \psi_{k,m} \in [0, \ 2\pi], \ \forall k, m, \quad (22)$$

$$\left\|\theta_{k,m}\right\| = 1, \ \forall k, m. \quad (23)$$

Due to the TDMA mode, the above problem can be decomposed into the following K separate sub-problems

$$\mathcal{P}1_{\mathbf{\Theta}_k}: \max_{\mathbf{\Theta}_k} \frac{\tau}{t} R_k, \quad (24)$$

$$\text{s.t.} \ \ \psi_{k,m} \in [0, \ 2\pi], \ \forall m, \quad (25)$$

$$\left\|\theta_{k,m}\right\| = 1, \ \forall m, \quad (26)$$

for $1 \le k \le K$.

2.1) Continuous Phase Shifts: The non-convex unit modulus constraint (26) can be relaxed as

$$\left\|\theta_{k,m}\right\| \leq 1,\ \forall\, k, m, \tag{27}$$

which is convex. In addition, $\left|\mathbf{v}_{k,i}^{\mathrm{T}}\boldsymbol{\Theta}_k\mathbf{G}_k\mathbf{f}_k\right|^2$ is a convex quadratic function of $\boldsymbol{\Theta}_k$, and by applying SCA, it can be approximated by the first-order Taylor expansion. Specifically, given local point $\boldsymbol{\Theta}_k^r$ in the r-th iteration, the following relationship holds

$$\begin{aligned}\sum_{i=1}^{N}\left|\mathbf{v}_{k,i}^{\mathrm{T}}\boldsymbol{\Theta}_k\mathbf{G}_k\mathbf{f}_k\right|^2 \geq &-\sum_{i=1}^{N}\left|\mathbf{v}_{k,i}^{\mathrm{T}}\boldsymbol{\Theta}_k^r\mathbf{G}_k\mathbf{f}_k\right|^2\\ &+2\Re\Big\{\sum_{i=1}^{N}\left(\mathbf{v}_{k,i}^{\mathrm{T}}\boldsymbol{\Theta}_k^r\mathbf{G}_k\mathbf{f}_k\right)^{\mathrm{H}}\left(\mathbf{v}_{k,i}^{\mathrm{T}}\boldsymbol{\Theta}_k\mathbf{G}_k\mathbf{f}_k\right)\Big\},\end{aligned} \tag{28}$$

which is linear and convex. As a result, $\mathcal{P}1_{\boldsymbol{\Theta}_k}$ can be approximated as a convex problem, which can be solved by an interior-point method [30]. Therefore, we can obtain the optimal phase shift vector $\boldsymbol{\varphi}_k^\star$ for each cluster, with $\boldsymbol{\varphi}_k^\star = \left[\varphi_{k,1}^\star, \varphi_{k,2}^\star, \ldots, \varphi_{k,M}^\star\right]$.

2.2) Discrete Phase Shifts: Since it is challenging to realize continuous amplitude phase-shift values in practice, we quantize the obtained solutions to the discrete values within the intervals of length $\Delta = \frac{2\pi}{2^e-1}$. Let $l_m = \left\lfloor \frac{\varphi_{k,m}^\star}{\Delta} \right\rfloor$. Then $\varphi_{k,m}^\star \in \left[l_m\Delta,\ (l_m+1)\Delta\right]$. The search space for the M discrete phase shifts comprises 2^M possibilities. To select the optimal discrete phase shift set from them, a decision method based on the BB algorithm is proposed.

As shown in Algorithm 1, we input the optimal continuous phase shift vector $\boldsymbol{\varphi}_k^\star$, an initial feasible discrete solution $\boldsymbol{\psi}_k^0 = \left[\psi_{k,1}^0, \ldots, \psi_{k,M}^0\right]$ and the corresponding throughput q_k^L as the lower bound of $\mathcal{P}1$. Besides, $\boldsymbol{\psi}_k^\star$ is initialized as an empty set to store the optimal discrete phase shifts. Next, starting from $m = 1$, the algorithm calls function BRANCH(m) (line 13 of Algorithm 1) to traverse feasible discrete phase shifts and find the optimal solution. For current element m, BRANCH(m) considers its two possible values iteratively. Note that in each loop, the following two cases are considered.

a) When m arrives at the final element, a complete set of phase shift values is obtained and the corresponding throughput q_k is obtained. Then it is compared with the current lower bound, and if $q_k > q_k^L$, q_k^L is updated to $q_k^L = q_k$ and terminate BRANCH(m).

b) When m has not reached M, we calculate q_k^U (the upper bound of the throughput) by relaxing the phase shifts from m to M to continuous values in $\boldsymbol{\psi}$ (denoted as $\widetilde{\boldsymbol{\psi}}$). If $q_k^U > q_k^L$, call function BRANCH(m+1); otherwise, terminate this path.

The above procedure iterates until all the possible paths are tried, after which the optimal discrete-valued phase shift vector $\boldsymbol{\psi}_k^\star$ and the corresponding maximum throughput q_k^L are returned. The worst-case computation complexity of this algorithm is on the order of $\mathsf{O}\big(2^M\big)$.

3) Alternating Optimization: Based on the solutions of Subsections IV-A1 and IV-A2, we devise an alternating optimization (AO) method to solve the optimization problem $\mathcal{P}1$, as summarized in Algorithm 2. To begin with, we fix the transmit power to $\overline{\mathbf{p}}$, and initialize $\mathbf{f}^0$ and $\boldsymbol{\psi}^0$ as well as calculate the corresponding throughput q^0. Furthermore, stopping criterion δ is set and iteration count is initialized to $s = 0$. In each loop, first $\mathbf{f}_k^{s+1}$ of each cluster is calculated by the closed-form solution (20) with fixed $\boldsymbol{\psi}^s$. Then with fixed $\mathbf{f}^{s+1}$, the continuous phase shifts are obtained by optimizing the convex approximation of the optimization $\mathcal{P}1_{\boldsymbol{\Theta}_k}$, based on which the discrete $\boldsymbol{\psi}^{s+1}$ are obtained using Algorithm 1. Lastly, the corresponding throughput is calculated. The iteration procedure is terminated when the throughput difference between two successive iterations is smaller than δ, yielding the optimal solution $\left(\mathbf{f}^\star, \boldsymbol{\psi}^\star, q^\star\right)$. The discussions on the

Algorithm 1: BB-based Phase Shift Algorithm

Input: The optimal continuous phase shift vector $\boldsymbol{\varphi}_k^*$, A feasible solution of discrete phase shift vector $\boldsymbol{\psi}_k^0$ and the corresponding throughput q_k^L;
Initialization: The optimal discrete phase shift vector $\boldsymbol{\psi}_k^\star \leftarrow \emptyset$;

1 **function** BRANCH(m)
2 **for** $j = 0 : 1$ **do**
3 $\psi_{k,m} = (l_m + j)\Delta$;
4 **if** $m = M$ **then**
5 Calculate the corresponding throughput q_k;
6 **if** $q_k > q_k^L$ **then**
7 $q_k^L = q_k$;
8 $\boldsymbol{\psi}_k^\star$ is the set of all phase shift values at current path;
9 **else**
10 Calculate $q_k^U = \max\limits_{\widetilde{\boldsymbol{\psi}}} \frac{\tau}{t} R_k$;
11 **if** $q_k^U > q_k^L$ **then**
12 Call BRANCH(m+1);
13 BRANCH(1);
14 **return** $\boldsymbol{\psi}_k^\star$, q_k^L.

Algorithm 2: Alternating Optimization for Solving $\mathcal{P}1$

Initialization: $\overline{\mathbf{p}} = \left[\overline{P}, \overline{P}, \ldots, \overline{P}\right]$, $\mathbf{f}^0 = \left[\mathbf{f}_1^0, \mathbf{f}_2^0, \ldots, \mathbf{f}_K^0\right]$, $\boldsymbol{\psi}^0 = \left[\boldsymbol{\psi}_1^0, \boldsymbol{\psi}_2^0, \ldots, \boldsymbol{\psi}_K^0\right]$, corresponding throughput q^0, stopping criterion $\delta = 10^{-3}$, iteration count $s = 0$;

1 **do**
2 **for** $k = 1 : K$ **do**
3 Update beamforming vector $\mathbf{f}_k^{s+1}$ by Eq. (20) with given $\boldsymbol{\psi}_k^s$;
4 **for** $k = 1 : K$ **do**
5 Obtain optimal continuous phase shifts using interior-point method [30] with given $\mathbf{f}_k^{s+1}$;
6 Calculate discrete phase shift vector $\boldsymbol{\psi}_k^{s+1}$ by Algorithm 1;
7 Calculate q^{s+1} with given $\overline{\mathbf{p}}$, $\mathbf{f}^{s+1}$ and $\boldsymbol{\psi}^{s+1}$;
8 **while** $|q^{s+1} - q^s| \geq \delta$;
9 **return** $\mathbf{f}^\star = \mathbf{f}^s$, $\boldsymbol{\psi}^\star = \boldsymbol{\psi}^s$ and throughput $q^\star = q^s$.

convergence and complexity of Algorithm 2 is given below.

3.1) Convergence: Denote the throughput at the s-th iteration as $q^s = q\left(\overline{\mathbf{p}}, \mathbf{f}^s, \boldsymbol{\psi}^s\right)$, where $\overline{\mathbf{p}}$, $\mathbf{f}^s$, $\boldsymbol{\psi}^s$ are the input of next iteration. As steps 2-3 solve the optimal beamforming vector $\mathbf{f}_k^{s+1}$ for each cluster, $q\left(\overline{\mathbf{p}}, \mathbf{f}^s, \boldsymbol{\psi}^s\right) \leq q\left(\overline{\mathbf{p}}, \mathbf{f}^{s+1}, \boldsymbol{\psi}^s\right)$ holds. Then steps 4-6 update the phase shift vector for each cluster into $\boldsymbol{\psi}_k^{s+1}$ based on $\mathbf{f}^{s+1}$, and the resulting $q\left(\overline{\mathbf{p}}, \mathbf{f}^{s+1}, \boldsymbol{\psi}^{s+1}\right)$ satisfies the following inequality

$$q\big(\overline{\mathbf{p}}, \mathbf{f}^s, \boldsymbol{\psi}^s\big) \leq q\big(\overline{\mathbf{p}}, \mathbf{f}^{s+1}, \boldsymbol{\psi}^s\big) \leq q\big(\overline{\mathbf{p}}, \mathbf{f}^{s+1}, \boldsymbol{\psi}^{s+1}\big), \quad (29)$$

which indicates that the objective function is non-decreasing in the consecutive iterations. Since the throughput is upper-bounded by a finite value due to the power constraint, we conclude that Algorithm 2 converges.

3.2) Complexity: In each iteration of Algorithm 2, the optimal beamforming is given by the closed form and its computational complexity is negligible. The main computational complexity $\mathsf{O}\left(\mathcal{N}^{3.5} + 2^M\right)$ comes from solving the optimal discrete phase shifts (steps 4-6), where $\mathcal{N}$ denotes the number of variables utilized by the interior-point method. As the iteration is conducted for s times, the total complexity of Algorithm 2 is $\mathsf{O}\left(s\big(\mathcal{N}^{3.5} + 2^M\big)\right)$.

B. Stage two: Power Allocation and Throughput Maximization

Because the CSI may change significantly over the transmission duration of t or K frames, we execute the power allocation every l frames given the beamformers and IRS phase shifts obtained in Stage one, where l is chosen such that the CSI remains approximately unchanged over the duration of $l\tau$. Obviously, the power allocation among l clusters can be reduced to the following optimization problem

$$\max_{\mathbf{p}_l} \sum_{k=\rho+1}^{\rho+l} \frac{\tau}{t} \log_2\left(1 + P_k \sum_{i=1}^{N} \frac{|\mathbf{v}_{k,i}^{\mathrm{T}} \boldsymbol{\Theta}_k \mathbf{G}_k \mathbf{f}_k|^2}{\sigma^2}\right), \quad (30)$$

$$\text{s.t.} \sum_{k=\rho+1}^{\rho+l} P_k = l\overline{P}, \quad (31)$$

$$0 \leq P_k \leq l\overline{P},\ \rho+1 \leq k \leq \rho+l, \quad (32)$$

where $\mathbf{p}_l = \left[P_{\rho+1}, \ldots, P_{\rho+l}\right]^{\mathrm{T}}$ is the power allocation vector for the current l frames, and ρ is the number of clusters whose power allocations have been executed. Note that we have set the total power consumption for every l frames to $l\overline{P} = \frac{l}{K} P_{\mathrm{sum}}$. As (30) is convex with respect to P_k and all the constraints are linear, this optimization is convex and can be solved by the Lagrangian multiplier method. Specifically, the Lagrangian function can be expressed as

$$L\left(\mathbf{p}_l, \boldsymbol{\lambda}, \boldsymbol{\beta}, \mu\right) = \sum_{k=\rho+1}^{\rho+l} -R_k - \lambda_k P_k - \beta_k\big(l\overline{P} - P_k\big) - \mu\left(\sum_{k=\rho+1}^{\rho+l} P_k - l\overline{P}\right), \quad (33)$$

where $\boldsymbol{\lambda} = \left[\lambda_{\rho+1}, \ldots, \lambda_{\rho+l}\right]^{\mathrm{T}}$ and $\boldsymbol{\beta} = \left[\beta_{\rho+1}, \ldots, \beta_{\rho+l}\right]^{\mathrm{T}}$ are the Lagrangian multipliers associated with the constraints (32), while μ is the Lagrangian multiplier associated with the constraint (31).

The Karush-Kuhn-Tucker (KKT) condition of (33) associated with P_k is given by

$$\frac{\partial L\left(\mathbf{p}_l, \boldsymbol{\lambda}, \boldsymbol{\beta}, \mu\right)}{\partial P_k} = -\frac{\frac{\sum_{i=1}^{N} |\mathbf{v}_{k,i}^{\mathrm{T}} \boldsymbol{\Theta}_k \mathbf{G}_k \mathbf{f}_k|^2}{\sigma^2}}{\ln 2\left(1 + P_k \frac{\sum_{i=1}^{N} |\mathbf{v}_{k,i}^{\mathrm{T}} \boldsymbol{\Theta}_k \mathbf{G}_k \mathbf{f}_k|^2}{\sigma^2}\right)} - \lambda_k + \beta_k - \mu = 0,\ \rho+1 \leq k \leq \rho+l. \quad (34)$$

An iterative gradient descent procedure can be utilized to obtain the optimal solutions $P_k^\star$, $\lambda_k^\star$, $\beta_k^\star$ and $\mu^\star$ based on the KKT conditions of (33) associated with P_k, λ_k, β_k and μ. Let λ_k^r, β_k^r and μ_k^r be the Lagrangian multiplier solutions after the r-th iteration. From (34), the power allocation solution P_k^r, $\rho+1 \leq k \leq \rho+l$, after the r-th iteration, can be obtained in the closed-form as

$$P_k^r = \frac{1}{\ln 2\big(\beta_k^r - \lambda_k^r - \mu^r\big)} - \frac{\sigma^2}{\sum_{i=1}^{N} \left|\mathbf{v}_{k,i}^{\mathrm{T}} \boldsymbol{\Theta}_k \mathbf{G}_k \mathbf{f}_k\right|^2}. \quad (35)$$

Then the Lagrangian multipliers are updated according to the associated KKT conditions as

$$\lambda_k^{r+1} = \lambda_k^r - c_k^r P_k^r,\ \rho+1 \leq k \leq \rho+l \quad (36)$$

$$\beta_k^{r+1} = \beta_k^r - d_k^r\big(l\overline{P} - P_k^r\big),\ \rho+1 \leq k \leq \rho+l \quad (37)$$

$$\mu^{r+1} = \mu^r - e^r\left(\sum_{k=\rho+1}^{\rho+l} P_k^r - l\overline{P}\right), \quad (38)$$

where c_k^r, d_k^r and e^r denote the corresponding step sizes.

Algorithm 3 summarizes the proposed power allocation procedure for throughput maximization based on the Lagrangian multiplier method. For notation convenience, we still denote the optimal beamformers and IRS phase shifts of the users

Algorithm 3: Power Allocation for Throughput Maximization

Input: Optimal beamformers and IRS phase shifts of the users in every l clusters $\mathbf{f}^\star$ and $\boldsymbol{\psi}^\star$;
Initialization: Maximum iteration times $r_{\max} = 100$, $\boldsymbol{\lambda}^0$, $\boldsymbol{\beta}^0$, $\boldsymbol{c}^0$, $\boldsymbol{d}^0$, $\mu^0 = 50$, $e^0 = 10$, stopping criterion $\varepsilon = 10^{-2}$, iteration index $r = 0$;

```
while r ≤ r_max do
    Calculate p_l^r with (35);
    Update λ^r, β^r, μ^r with (36)-(38);
    if any of c_i^r, d_i^r, e^r > 1 then
        Decrease its value by half in the next iteration;
    if ‖λ^{r+1} − λ^r‖ < ε and ‖β^{r+1} − β^r‖ < ε and |μ^{r+1} − μ^r| < ε then
        break;
    r = r + 1;
Calculate the optimal throughput q(p_l^⋆ = p_l^r, f^⋆, ψ^⋆);
return p_l^⋆, q(p_l^⋆, f^⋆, ψ^⋆).
```

in every l clusters obtained in Stage One by $\mathbf{f}^\star$ and $\boldsymbol{\psi}^\star$, which together with the maximum iteration times $r_{\max}$ and stopping criterion ε are inputted to the algorithm. Also, the initial values of Lagrangian multipliers and the corresponding gradient descent step sizes are given. In each iteration, each P_k is calculated by (35) in line 2, and the Lagrangian multipliers are updated according to (36)-(38) in line 3. Then the step sizes are adjusted appropriately in lines 4-5. After convergence, the optimal power allocation vector $\mathbf{p}_l^\star$ and the corresponding throughput $q\left(\mathbf{p}_l^\star, \mathbf{f}^\star, \boldsymbol{\psi}^\star\right)$ are returned.

Observe that the step sizes in Algorithm 3 remain positive and non-increasing over the iteration procedure. More importantly, due to the convexity of the problem (30)-(32), the KKT point is also the global optimal solution in the l frames. Executing this algorithm for $\frac{K}{l}$ times, we obtain the total power allocation for the entire transmission period.

V. Performance Evaluation

We provide numerical simulation results to verify the effectiveness of our proposed IRS assisted throughput maximization approach for mmWave HST communication systems.

A. Simulation Setup

Unless otherwise stated, the simulation system's parameters used are listed in Table I. With reference to [31]–[33], the simulated HST communication system operates at 28 GHz, with signal attenuation $h_0 = -61.3849$ dB at 1 m reference distance. The IRS is a uniform square array of 64 elements, with the element spacing being half the wavelength. The number of BS transmit antennas is 16, with the antenna spacing being half the wavelength. The locations of communication nodes are represented by three-dimensional (3D) coordinates. Specifically, we fix the BS at $(20, 0, 2)$, place the IRS on the YZ plane at the height of 1 m, i.e., at $(0, 0, 1)$, and update the positions of IRS and users frame by frame. All the simulation results are averaged over 200 independent experiments.

TABLE I
Default System Parameters

Parameter	Symbol	Value
Frame duration	τ	0.1 s
Carrier frequency	f	28 GHz
Coverage radius of the cell	R	1 km
Distance between BS and rail	D_0	20 m
Average transmit power	$\overline{P}$	20 dBm
Number of BS antennas	L	16
IRS elements	M	64
System bandwidth	W	2000 MHz
Background noise	N_0	-80 dBm/Hz
Rician K-factor	K_f	3 dB
PL factor of BS-IRS links	β_1	2 dB
PL factor of IRS-user links	β_2	3 dB
Speed of HST	v	300 km/h
Length of power allocation	l	10
Phase shift quatization bits	e	2
Total number of users served	I	400

Four existing schemes are utilized for performance comparison with our proposed approach, which include

- **Neighbor-based Cross-entropy (NCE)** [32]: This low-complexity algorithm selects phase shifts of the IRS in the candidate set, which is generated based on the probability distribution function and extended through neighbor extraction.
- **Successive Refinement (SR)** [23], [34]: This scheme considers the suboptimal zero-forcing (ZF) beamforming at the BS and alternately optimizes the phase shift of each programmable element by fixing the others.
- **Random Phase Shift (RPS)**: This scheme randomly selects a feasible phase shift for each IRS element.
- **Without-RIS**: This scheme does not consider the assistance of IRS, and on-board users can only receive signals going through the carriage.

B. The effect of IRS adoption

In this subsection, we evaluate the sum-rate of users in one frame to demonstrate the effect of IRS deployment and compare the performance of the five schemes by varying the number of users, the number of IRS elements, the K-factor and the quantification bits e, respectively. In the experiments, users are distributed randomly in the carriage. Note that the sum-rate is the throughput in one frame.

In Fig. 3, we plot the sum-rates achieved by the five schemes as the functions of the number of users per cluster N. Observe that the sum rate increases logarithmically with N, and our scheme outperforms the other four schemes. At $N = 10$, the performance gains of our scheme over the NCE, SR and RPS are around 3.7%, 6.9% and 12.9%, respectively, which clearly demonstrates the design benefits of jointly optimizing beamforming and phase shifts. Furthermore, at $N = 10$, our scheme outperforms the scheme without IRS by 20.1%, which confirms the effectiveness of the window-deployed IRS.

Fig. 4 illustrates the influence of IRS size on the throughput performance of the five schemes, by varying the number of IRS elements M from 64 to 320. As expected, the four

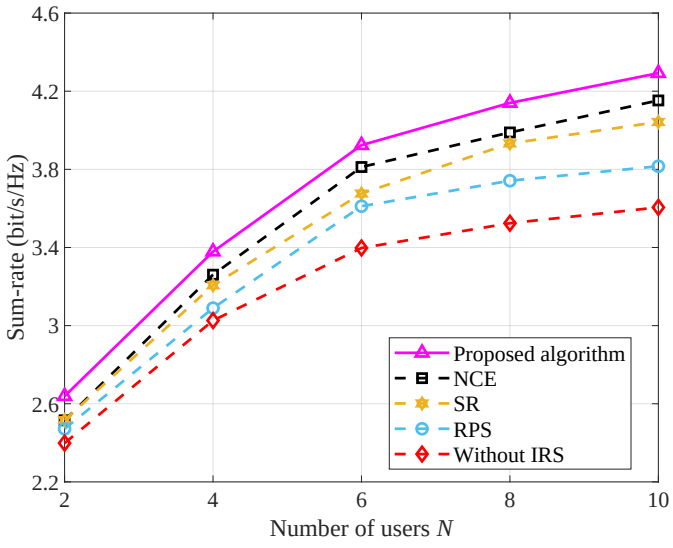

Fig. 3. Sum rate versus the number of users per frame.

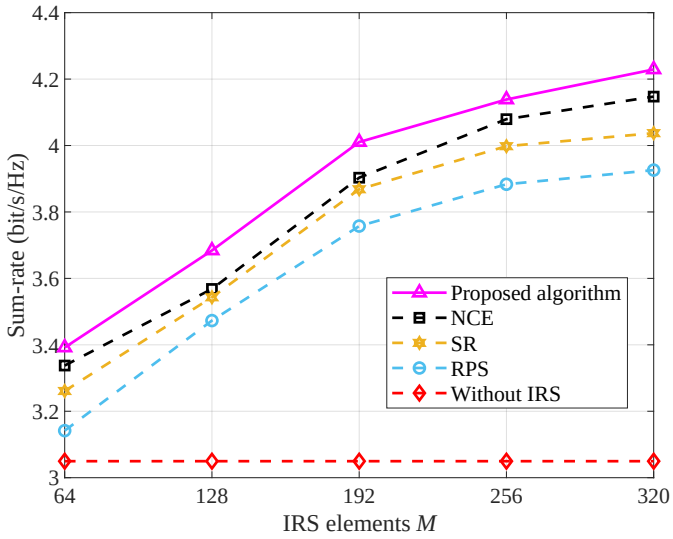

Fig. 4. Sum rate versus the number of IRS elements.

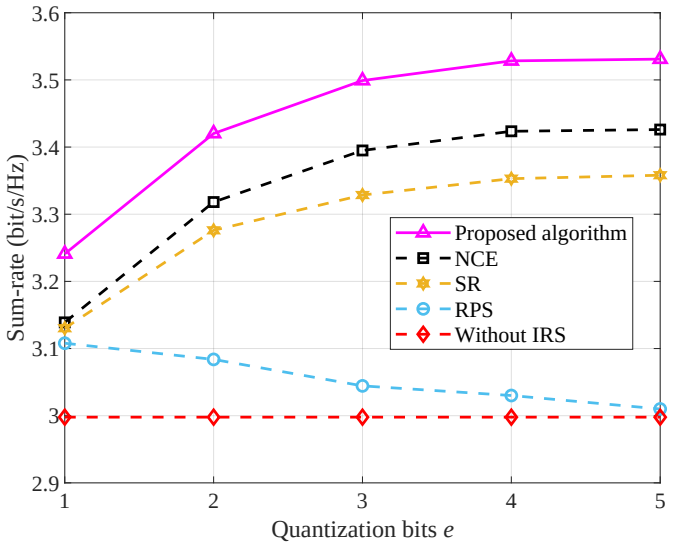

Fig. 6. Sum rate versus quantification bits.

schemes with IRS significantly outperform the scheme without IRS, and their sum-rate performance increase with M, since more RIS elements result in sharper beams which refract incident signals towards desired devices and mitigate interferences among users more effectively. Again our scheme achieves the best performance. It can be seen from Fig. 4 that the performance gap between our proposed scheme and the second-best NCE is 0.15 bit/s/Hz to 0.1 bit/s/Hz for $128 \leq M \leq 320$. But the NCE algorithm offers the advantage of low complexity.

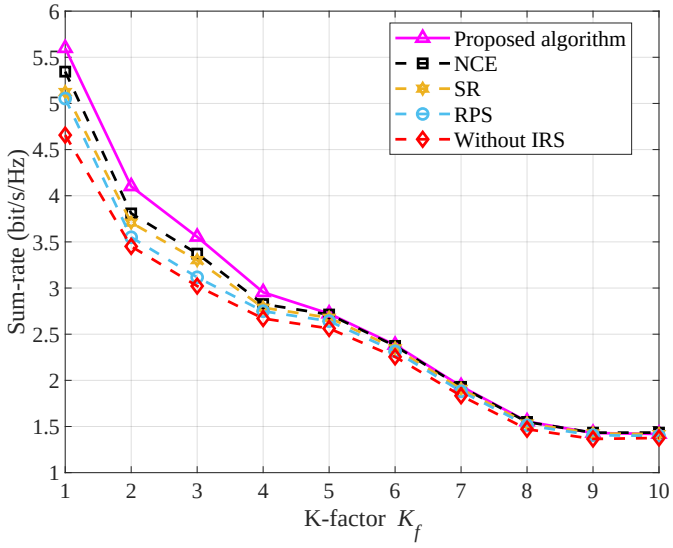

Fig. 5. Sum rate versus K-factor.

Fig. 5 shows the impact of Rician K-factor on the achievable sum-rates of the five schemes. Observe that the sum rate is a decreasing function with respect to K_f, and the performance gap among the five schemes becomes negligible when $K_f \geq 5$. This is because as K_f increases, the LoS path becomes stronger while the adjustable multipaths decrease, thus limiting the capacity improvement obtained through IRS deployment. Considering the characteristics of railway communication, $K_f = 3$ or 4 is typical in practice [35].

Fig. 6 compares the sum-rates of the five schemes at different quantization bits e. As expected, the proposed algorithm attains the best performance and the curve without IRS stays flat. Moreover, the achievable rates of the proposed, NCE and SR schemes first increase with e and then reach their respectively saturation values of 3.53 bit/s/Hz, 3.42 bit/s/Hz and 3.36 bit/s/Hz when the number of quantization bits e exceeds 4. By contrast, the performance of the RPS decreases as e increases, and becomes close to that of the scheme without-IRS at $e = 5$. The reason is that RPS adjusts the phase shift of each element in a completely random manner, and the adjusted signal is not necessarily stronger than the incident signal. Evidently, IRS deployment with suitable optimization and quantization bits enables higher network throughput.

C. The overall throughput

Next we evaluate the achievable overall throughput of the proposed algorithm, the NCE, SR and RPS schemes as well as the scheme without-IRS. Fig. 7 depicts the average throughput of these five schemes as the functions of the HST speed v in time duration t, given the default system parameters of $N = 4$,

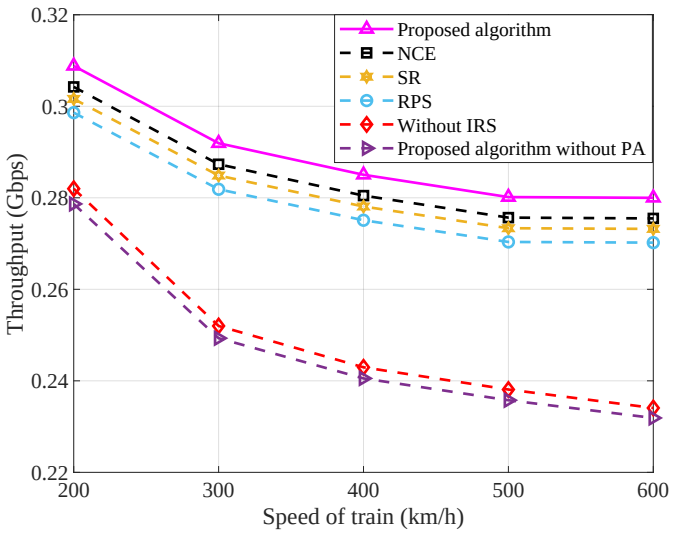

Fig. 7. Achievable throughput versus mobility speed.

$M = 64$, $e = 2$ and $K_f = 3$. As expected, the throughput of all the five schemes decrease as v increases, and the proposed scheme attains the best performance.

As explained in Section IV, our proposed scheme consists of two stages, with the stage one performing joint optimization of beamforming and IRS phase shifts, while the stage two carrying out power allocation for throughput maximization based on the results of the stage one. The proposed power allocation, namely, Algorithm 3, is crucial for maximizing the throughput. To demonstrate the effectiveness of Algorithm 3, in Fig. 7, we also plot the average throughput achieved by performing the stage-one optimization only with equal power allocation, denoted as the proposed algorithm without power allocation. It can be seen that the proposed power allocation algorithm significantly improves the system throughput, and it outperforms the scheme without power allocation by 10.4% at $v = 200$ km/h and by 20.7% at $v = 600$ km/h.

VI. Conclusions

In this paper, we have considered the downlink communication in an IRS-assisted mmWave HST system, where user clustering and hybrid TDMA-NOMA technique are leveraged to mitigate transmission interference. To enhance the communication quality of on-board services, our main contribution has been to formulate the throughput maximization problem and propose a two-stage solution. In stage one, beamforming and phase shift are alternately optimized frame by frame. Specifically, given the fixed phase shifts, the optimal beamforming is enabled by MRT, after which phase shifts are optimized with SCA and the BB algorithm. Then in stage two, based on the results of stage one, the power allocation is performed to maximize the overall throughput. Numerical simulation results have verified the effectiveness of IRS adoption and confirmed the superior performance of the proposed algorithm over existing solutions. Furthermore, the results have demonstrated that the proposed power allocation algorithm in stage two significantly improves the system throughput.

References

[1] B. Jones, *Past, present and future: The evolution of China's incredible high-speed rail network*, CNN Travel, Feb. 9, 2022. [Online]. Available: https://edition.cnn.com/travel/article/china-high-speed-rail-cmd/index.html

[2] R. He, *et al.*, "High-speed railway communications: From GSM-R to LTE-R," *IEEE Vehicular Technology Mag.*, vol. 11, no. 3, pp. 49–58, Sep. 2016.

[3] Y. Liu, C.-X. Wang, and J. Huang, "Recent developments and future challenges in channel measurements and models for 5G and beyond high-speed train communication systems," *IEEE Communi. Mag.*, vol. 57, no. 9, pp. 50–56, Sep. 2019.

[4] B. Ai, *et al.*, "Future railway services-oriented mobile communications network," *IEEE Communi. Mag.*, vol. 53, no. 10, pp. 78–85, Oct. 2015.

[5] R. He, *et al.*, "5G for railways: The next generation railway dedicated communications," *IEEE Communi. Mag.*, Early Access, Sep. 19, 2022. DOI:10.1109/MCOM.005.2200328

[6] T. Bai and R. W. Heath, "Coverage analysis for millimeter wave cellular networks with blockage effects," in *Proc. IEEE GlobalSIP 2013* (Austin, TX, USA), Dec. 3-5, 2013, pp. 727–730.

[7] J. Zhang, *et al.*, "RIS-aided next-generation high-speed train communications: Challenges, solutions, and future directions," *IEEE Wireless Communi.*, vol. 28, no. 6, pp. 145–151, Dec. 2021.

[8] H. Song, X. Fang, and Y. Fang, "Millimeter-wave network architectures for future high-speed railway communications: Challenges and solutions," *IEEE Wireless Communi.*, vol. 23, no. 6, pp. 114–122, Dec. 2016.

[9] Y. Zhou and B. Ai, "Handover schemes and algorithms of high-speed mobile environment: A survey" *Computer Communi.*, vol. 47, pp. 1–15, Jul. 2014.

[10] Y. Youn, *et al.*, "Demo: Transparent intelligent surfaces for sub-6 GHz and mmWave B5G/6G systems," in *Proc. ICC Workshops 2022* (Seoul, Korea), May 16-20, 2022, pp. 1–2.

[11] M. Hua and Q. Wu, "Joint dynamic passive beamforming and resource allocation for IRS-aided full-duplex WPCN," *IEEE Trans. Wireless Communi.*, vol. 21, no. 7, pp. 4829–4843, Jul. 2022.

[12] M. Hua, *et al.*, "Intelligent reflecting surface-aided joint processing coordinated multipoint transmission," *IEEE Trans. Communi.*, vol. 69, no. 3, pp. 1650–1665, Mar. 2021.

[13] D. Kitayama, *et al.*, "Transparent dynamic metasurface for a visually unaffected reconfigurable intelligent surface: Controlling transmission/reflection and making a window into an RF lens," *Opt. Express*, vol. 29, no. 18, pp. 29292–29307, Aug. 2021.

[14] Z. Ma, *et al.*, "Interference suppression for railway wireless communication systems: A reconfigurable intelligent surface approach," *IEEE Trans. Vehicular Technology*, vol. 70, no. 11, pp. 11593–11603, Nov. 2021.

[15] J. Xu and B. Ai, "When mmWave high-speed railway networks meet reconfigurable intelligent surface: A deep reinforcement learning method," *IEEE Wireless Communi. Letters*, vol. 11, no. 3, pp. 533–537, Mar. 2022.

[16] Y. M. Park, Y. K. Tun, Z. Han, and C. S. Hong, "Trajectory optimization and phase-shift design in IRS assisted UAV network for high speed trains," *arXiv:2107.00857*, 2021.

[17] M. Gao, *et al.*, "IRS-assisted high-speed train communications: Outage probability minimization with statistical CSI," in *Proc. ICC 2021* (Montreal, QC, Canada), Jun 14-23,. 2021, pp. 1–6.

[18] T. Li, *et al.*, "Double IRSs aided massive MIMO channel estimation and spectrum efficiency maximization for high-speed railway communications," *IEEE Trans. Vehicular Technology*, vol. 71, no. 8, pp. 8630–8645, Aug. 2022.

[19] J. P. S. Wong, A. Epstein, and G. V. Eleftheriades, "Reflectionless wide-angle refracting metasurfaces," *IEEE Antennas and Wireless Propagation Letters*, vol. 15, pp. 1293–1296, 2016.

[20] V. S. Asadchy, *et al.*, "Perfect control of reflection and refraction using spatially dispersive metasurfaces," *Physical Review B*, vol. 94, pp. 075142-1–075142-14, Aug. 2016.

[21] Z. Huang, B. Zheng, and R. Zhang, "Transforming fading channel from fast to slow: Intelligent refracting surface aided high-mobility communication," *IEEE Trans. Wireless Communi.*, vol. 21, no. 7, pp. 4989–5003, Jul. 2022.

[22] Y. Wang, *et al.*, "Doppler shift and channel estimation for intelligent transparent surface assisted communication systems on high-Speed railways," *arXiv:2208.00455*, 2022.

[23] S. Zhang, *et al.*, "Intelligent omni-surfaces: Ubiquitous wireless transmission by reflective-refractive metasurfaces," *IEEE Trans. Wireless Communi.*, vol. 21, no. 1, pp. 219–233, Jan. 2022.

[24] X. Cao, *et al.*, "Reconfigurable intelligent surface-assisted aerial-terrestrial communications via multi-task learning," *IEEE J. Sel. Areas Communi.*, vol. 39, no. 10, pp. 3035–3050, Oct. 2021

[25] Y. Liu, *et al.*, "Developing NOMA to next generation multiple access (NGMA): Future vision and research opportunities," *IEEE Wireless Communi.*, Early Access, Jun. 24, 2022, DOI:10.1109/MWC.007.2100553.

[26] F. Fang, *et al.*, "Joint user scheduling and power allocation optimization for energy-efficient NOMA systems with imperfect CSI," *IEEE J. Sel. Areas Communi.*, vol. 35, no. 12, pp. 2874–2885, Dec. 2017.

[27] Q. Wu, W. Chen, D. W. K. Ng, and R. Schober, "Spectral and energy-efficient wireless powered IoT networks: NOMA or TDMA?," *IEEE Trans. Vehicular Technology*, vol. 67, no. 7, pp. 6663–6667, Jul. 2018.

[28] D. Tse and P. Viswanath, *Fundamentals of Wireless Communication*. Cambridge, U.K.: Cambridge Univ. Press, 2005.

[29] Q. Wu and R. Zhang, "Intelligent reflecting surface enhanced wireless network via joint active and passive beamforming," *IEEE Trans. Wireless Communi.*, vol. 18, no. 11, pp. 5394–5409, Nov. 2019.

[30] S. Boyd and L. Vandenberghe, *Convex Optimization*. Cambridge, U.K.: Cambridge Univ. Press, 2014.

[31] D. Dampahalage, K. B. S. Manosha, N. Rajatheva, and M. Latva-aho, "Intelligent reflecting surface aided vehicular communications,"

in *Proc. Globecom Workshops 2020* (Taipei, Taiwan, China), Dec. 7-11, 2020, pp. 1–6.

[32] R. Su, *et al.*, "Capacity enhancement for irregular reconfigurable intelligent surface-aided wireless communications," in *Proc. Globecom 2020* (Taipei, Taiwan, China), Dec. 7-11, 2020, pp. 1–6.

[33] L. Wang, *et al.*, "Energy-efficient power control of train-ground mmWave communication for high-speed trains," *IEEE Trans. Vehicular Technology*, vol. 68, no. 8, pp. 7704–7714, Aug. 2019.

[34] Q. Wu and R. Zhang, "Beamforming optimization for wireless network aided by intelligent reflecting surface with discrete phase shifts," *IEEE Trans. Communi.*, vol. 68, no. 3, pp. 1838–1851, Mar. 2020.

[35] G. Li, *et al.*, "On the feasibility of high speed railway mmWave channels in tunnel scenario" *Wireless Communi. Mobile Computing*, vol. 2017, Article ID 7135896, pp. 1–17, Oct. 2017.

Jing Li received the M.E. degree from Beijing Jiaotong University, China, in 2020, where she is currently pursuing her Ph.D. degree. Her research interests include millimeter wave communications and medium access control.

Yong Niu (IEEE Member) received the B.E. degree in Electrical Engineering from Beijing Jiaotong University, China in 2011, and the Ph.D. degree in Electronic Engineering from Tsinghua University, Beijing, China, in 2016. His research interests are in the areas of networking and communications, including millimeter wave communications, device-to-device communication, medium access control, and software-defined networks. He is currently an Associate Professor with the State Key Laboratory of Rail Traffic Control and Safety, Beijing Jiaotong University. During November 2014 to April 2015, he visited University of Florida, FL, USA as a Visiting Scholar. He received the Ph.D. National Scholarship of China in 2015, Outstanding Ph. D Graduates and Outstanding Doctoral thesis of Tsinghua University in 2016, and Outstanding Ph. D Graduates of Beijing in 2016. He has served as Technical Program Committee (TPC) member for CHINACOM 2015 and IWCMC 2017, and also session chair for IWCMC 2017 and CHINACOM 2017.

Hao Wu (IEEE Member) received the Ph.D. degree in information and communication engineering from Harbin Institute of Technology in 2000. She is currently a full professor with the State Key Lab of Rail Traffic Control and Safety at Beijing Jiaotong University (BJTU), China. She has published more than 100 papers in international journals and conferences. Her research interests include Intelligent Transportation Systems (ITS), security and QoS issues in wireless networks (VANETs, MANETs and WSNs), wireless communications, and Internet of Things (IoT). She is a member of IEEE and a reviewer of its major conferences and journals in wireless networks and security.

Bo Ai (IEEE Fellow) received his M.S. and Ph.D. degrees from Xidian University, China, in 2002 and 2004, respectively. He is a full professor and Ph.D. degree candidate advisor with the State Key Laboratory of Rail Traffic Control and Safety at Beijing Jiaotong University, China. He is the deputy director of the State Key Laboratory of Rail Traffic Control and Safety. He has authored/co-authored six books and published over 230 academic research papers. He holds 21 invention patents. He is an Institution of Engineering and Technology fellow. He is an associate editor of IEEE Transactions on Consumer Electronics and an editorial committee member of Wireless Personal Communications.

Ruisi He (IEEE Senior Member) received the B.E. and Ph.D. degrees from Beijing Jiaotong University (BJTU), Beijing, China, in 2009 and 2015, respectively. Since 2015, he has been with the State Key Laboratory of Rail Traffic Control and Safety, BJTU, where he has been a Full Professor since 2018. He is a Visiting Scholar with the Georgia Institute of Technology, Atlanta, GA, USA, University of Southern California, Los Angeles, CA, USA, and Universit Catholique de Louvain, Belgium. He has authored or coauthored five books, three book chapters, more than 200 journal and conference papers, and also several patents. His research interests include wireless propagation channels, railway and vehicular communications, 5G and 6G communications. He is the Editor of the IEEE Transactions on Wireless Communications, the IEEE Antennas and Propagation Magazine, the IEEE Communications Letters, the IEEE Open Journal of Vehicular Technology, and a Lead Guest Editor of the IEEE Journal on Selected Area in Communications and the IEEE Transactions on Antennas and Propagation. He serves as the Early Career Representative (ECR) of Commission C, International Union of Radio Science (URSI). He was the recipient of the URSI Issac Koga Gold Medal in 2020, the IEEE ComSoc Asia-Pacific Outstanding Young Researcher Award in 2019, the URSI Young Scientist Award in 2015, and five best paper awards in conferences. He is a Member of the COST.

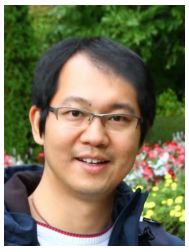

Ning Wang (IEEE Member) received the B.E. degree in communication engineering from Tianjin University, Tianjin, China, in 2004, the M.A.Sc. degree in electrical engineering from The University of British Columbia, Vancouver, BC, Canada, in 2010, and the Ph.D. degree in electrical engineering from the University of Victoria, Victoria, BC, Canada, in 2013. From 2004 to 2008, he was with the China Information Technology Design and Consulting Institute, as a Mobile Communication System Engineer, specializing in planning and design of commercial mobile communication networks, network traffic analysis, and radio network optimization. From 2013 to 2015, he was a Postdoctoral Research Fellow with the Department of Electrical and Computer Engineering, The University of British Columbia. Since 2015, he has been with the School of Information Engineering, Zhengzhou University, Zhengzhou, China, where he is currently an Associate Professor. He also holds adjunct appointments with the Department of Electrical and Computer Engineering, McMaster University, Hamilton, ON, Canada, and the Department of Electrical and Computer Engineering, University of Victoria, Victoria, BC, Canada. His research interests include resource allocation and security designs of future cellular networks, channel modeling for wireless communications, statistical signal processing, and cooperative wireless communications. He has served on the technical program committees of international conferences, including the IEEE GLOBECOM, IEEE ICC, IEEE WCNC, and CyberC. He was on the Finalist of the Governor Generals Gold Medal for Outstanding Graduating Doctoral Student with the University of Victoria in 2013.

Sheng Chen (IEEE Fellow) received his BEng degree from the East China Petroleum Institute, Dongying, China, in 1982, and his PhD degree from the City University, London, in 1986, both in control engineering. In 2005, he was awarded the higher doctoral degree, Doctor of Sciences (DSc), from the University of Southampton, Southampton, UK. From 1986 to 1999, He held research and academic appointments at the Universities of Sheffield, Edinburgh and Portsmouth, all in UK. Since 1999, he has been with the School of Electronics and Computer Science, the University of Southampton, UK, where he holds the post of Professor in Intelligent Systems and Signal Processing. Dr Chen's research interests include adaptive signal processing, wireless communications, modeling and identification of nonlinear systems, neural network and machine learning, intelligent control system design, evolutionary computation methods and optimization. He has published over 600 research papers. Professor Chen has 18,200+ Web of Science citations with h-index 59 and 35,600+ Google Scholar citations with h-index 81. Dr. Chen is a Fellow of the United Kingdom Royal Academy of Engineering, a Fellow of Asia-Pacific Artificial Intelligence Association and a Fellow of IET. He is one of the original ISI highly cited researchers in engineering (March 2004).